



**HAL**  
open science

## Smaller Diameter Optical Fibre Sensor for Automated Embedding in Composite Laminates

Eli Voet, Tahira Ahmed, Eric Lindner, Geert Luyckx, Anders Brodsjo, Joris Degrieck

► **To cite this version:**

Eli Voet, Tahira Ahmed, Eric Lindner, Geert Luyckx, Anders Brodsjo, et al.. Smaller Diameter Optical Fibre Sensor for Automated Embedding in Composite Laminates. EWSHM - 7th European Workshop on Structural Health Monitoring, IFFSTTAR, Inria, Université de Nantes, Jul 2014, Nantes, France. hal-01021043

**HAL Id: hal-01021043**

**<https://inria.hal.science/hal-01021043>**

Submitted on 9 Jul 2014

**HAL** is a multi-disciplinary open access archive for the deposit and dissemination of scientific research documents, whether they are published or not. The documents may come from teaching and research institutions in France or abroad, or from public or private research centers.

L'archive ouverte pluridisciplinaire **HAL**, est destinée au dépôt et à la diffusion de documents scientifiques de niveau recherche, publiés ou non, émanant des établissements d'enseignement et de recherche français ou étrangers, des laboratoires publics ou privés.

## SMALLER DIAMETER OPTICAL FIBRE SENSOR FOR AUTOMATED EMBEDDING IN COMPOSITE LAMINATES

Eli Voet<sup>1,2</sup>, Tahira Ahmed<sup>3</sup>, Eric Lindner<sup>2</sup>, Geert Luyckx<sup>1</sup>, Anders Brødsjø<sup>3</sup>, Joris Degrieck<sup>1</sup>

<sup>1</sup> UGent department of materials and engineering, Technologiepark 903 9052 Zwijnaarde, Belgium

<sup>2</sup> FBGS Technologies GmbH, Buchaer Strasse 6 D-07745 Jena, Germany

<sup>3</sup> Airborne Technology Centre Laan van Ypenburg 70 2497GB Den Haag, The Netherlands

eli.voet@ugent.be

### ABSTRACT

In the framework of the FP7-project SMARTFIBER (<http://www.smartfiber-fp7.eu/>) an optical fibre prototype has been developed with a cladding diameter of approximately 60 µm. Draw Tower fibre Bragg gratings (DTG®s) are inscribed in this fibre which show identical strain optic and thermo optic characteristics compared to the standard commercial available 125 µm version, moreover they show superb ultimate failure strain of more than 7%. This characteristic plays an important role when automatic fibre embedding processes are envisaged. In this paper, the developed 60 µm fibre prototypes are successfully been applied during automated fibre placement on prepreg material. The results of the calibration tests and of the strain evolution of the DTG® during automated fibre placement will be presented in this paper

**KEYWORDS :** *fibre Bragg gratings, automated fibre placement, embedded sensors, fibre reinforced composites, strain monitoring.*

### INTRODUCTION

SMARTFIBER is a EU FP7 funded research project aiming at implementing a smart miniaturized system for "health monitoring" of composite materials, which integrates optical fibre sensor technology, nano-photonics chip technology and low power wireless technology. The work presented in this paper focusses on the work package specific dealing with automatically embed small diameter fibre Bragg grating (FBG) sensors in composite materials. When an optical fibre is embedded in composite materials and is not properly designed, it can negatively affect its mechanical properties because of local stress concentrations and hence distortion of the material occurs.

To avoid these detrimental effects, the boundaries of the FBG technology is pushed by developing an FBG sensor with a reduced diameter, which will allow to minimize the impact of the embedded fibre on the mechanical properties of the composite material. This advanced sensor is being manufactured using an innovative full automatic production process from FBGS-Technologies GmbH (Jena), which allows writing Fibre Bragg Gratings during the drawing of the fibre (Draw Tower Gratings - DTG®s [1]).

A key issue when dealing with FBGs for in-situ health monitoring of composite materials, is the embedding strategy. Current (manual/semi-automated) methods for FBG embedding are labor intensive, and do not ensure a good placement repeatability which is required for a reliable and robust structural health monitoring system. For this reason, the feasibility of automatic embedding of the advanced thinner FBGs in composite material is explored by extending existing automatic fibre placement strategies, developed for composite manufacturing such as Automated Fibre Placement technology (AFP).

In this paper, the development, processing, and characterization of a 60  $\mu\text{m}$  diameter DTG® prototype is presented. First results of AFP using the 60  $\mu\text{m}$  prototypes are shown, proving the controllability and repeatability of this embedding strategy.

## 1 DESIGN AND PROCESSING OF THE 60 $\mu\text{m}$ DRAW TOWER FBG

During previous R&D work at FBGS-technologies GmbH it has been shown that it is feasible to produce DTG®s with a cladding diameter of 80  $\mu\text{m}$ . These fibres are commercially available today [1], however from experience gained during previous research during fibre drawing it is known that once the fibre is that thin the smallest misalignment and process instability can cause early failure and end of the process. In the next subsections, the manufacturing and characterization of 60  $\mu\text{m}$  prototype draw tower FBGs is elaborated.

### 1.1 Production of 60 $\mu\text{m}$ Silica optical fibre

During preliminary trials, the limits of the current fibre drawing installation in terms of fibre diameter were tested. It is found that between a fibre cladding diameter of 60  $\mu\text{m}$  and 40  $\mu\text{m}$  large fluctuations ( $\sim 5\text{-}10$   $\mu\text{m}$ ) occur in the outer diameter of the optical fibre, which, on its turn, lead to undesirable effects such as fibre vibrations, fibre pinching in the coating applicator and fibre breakage during the process. With the fibre cladding diameter set to 60  $\mu\text{m}$ , we have been able to draw successfully a few hundred meters of pure silica (dummy) fibre resulting in a stable cladding diameter of approximately 62  $\mu\text{m}$  and an outer diameter with ORMOCER® coating of approximately 106  $\mu\text{m}$  (Figure 1, left). This latter dimension is already very close to the thickness of a commonly used composite reinforcement layer (e.g. carbon prepregs or yarns) or smaller than commonly used glass fibre bundles, which improves the integration of the fibre optic sensors in between the reinforcement fibres.

An important factor with respect to testing and first read-out of the sensors is the splicing or connectorisation of the thinner fibre to a standard fibre pigtail. Splicing tests of the 62  $\mu\text{m}$  fibre to standard 125  $\mu\text{m}$  telecom fibre were successful with normal splice losses (Figure 1, right). However, it must be noted that only manual splicing tests were possible by using adapted splice programs. Additionally coating removal and cleaving of the fibre end facet is not common and needs some extra handling because standard commercial tools are not yet available for fibre diameters below 80 $\mu\text{m}$ .

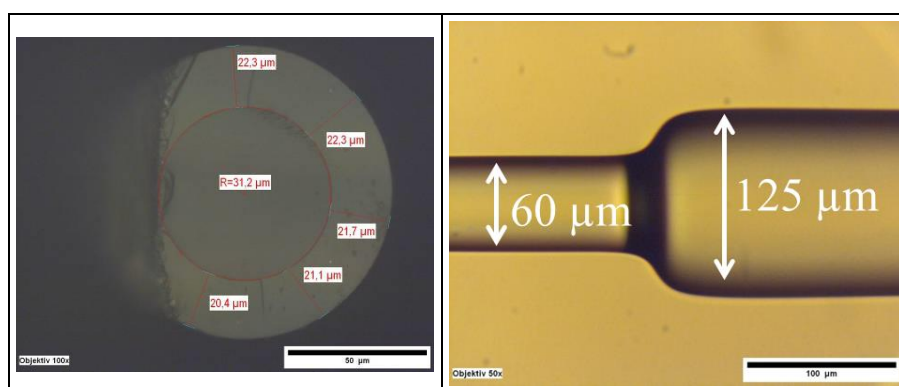


Figure 1: Pure silica fibre with a cladding diameter of 62  $\mu\text{m}$  and coating diameter of 106 $\mu\text{m}$  (left), Example of a spliced 62  $\mu\text{m}$  “dummy” fibre to a standard 125 $\mu\text{m}$  fibre (right).

### 1.2 Production of the first 60µm Draw Tower FBGs

In a second stage, using in this case a photosensitive fibre preform, we have succeeded in drawing fibre with a cladding of approximately 63 µm and an outer diameter with ORMOCER® coating of approximately 106 µm (Figure 2, left). This is similar to the result we obtained for the dummy fibre drawing using a pure silica preform. A small coating non-concentricity exists of approximately 2.5µm caused by a small misalignment between the fibre and centre of the coating applicator. Extra attention is needed to minimize this effect in future runs to avoid possible negative effects on the FBG response once embedded.

Similar to the dummy fibre, a manual splicing program is used to successfully splice 63 µm fibre with DTG®s to a standard 125 µm single mode fibre pigtail with FC/APC connector to be able to read out the sensors (Figure 2, right).

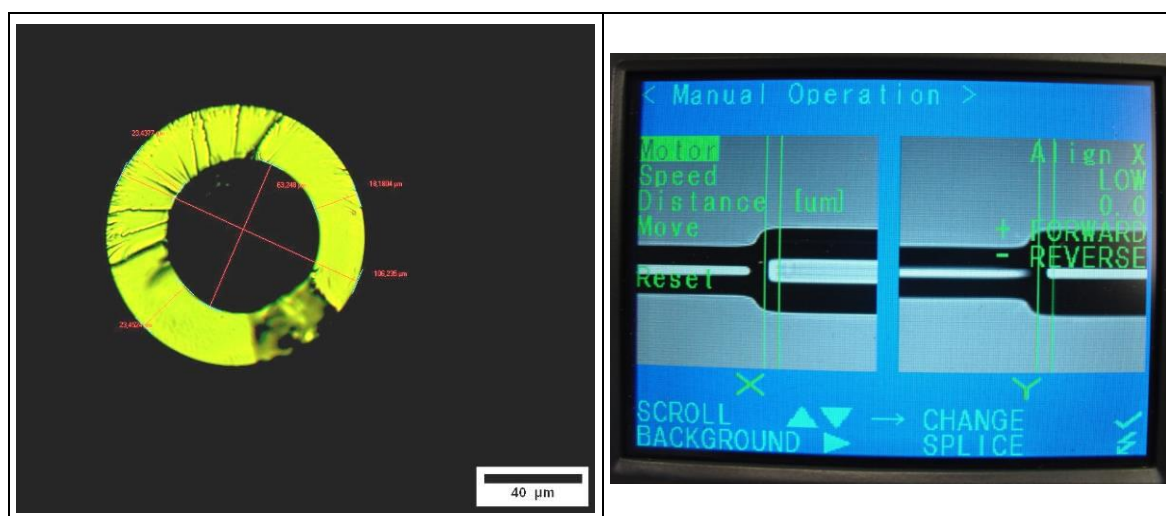


Figure 2: Cross section of the 63 µm DTG® fibre with ORMOCER® coating of approximately 106µm (left), Example of a spliced 63 µm DTG® fibre to a standard 125µm fibre (right).

During fibre drawing, several single DTG®s (Figure 3, left) and DTG® arrays (Figure 3, right) are inscribed. It is found that the spectral shape and FWHM (120pm) of all 63 µm versions is identical to that of standard DTG®s. More information regarding the assessment of the quality of these prototype DTG®s is found in Section 1.3, where the mechanical, opto-mechanical and thermo-optic sensor properties are determined.

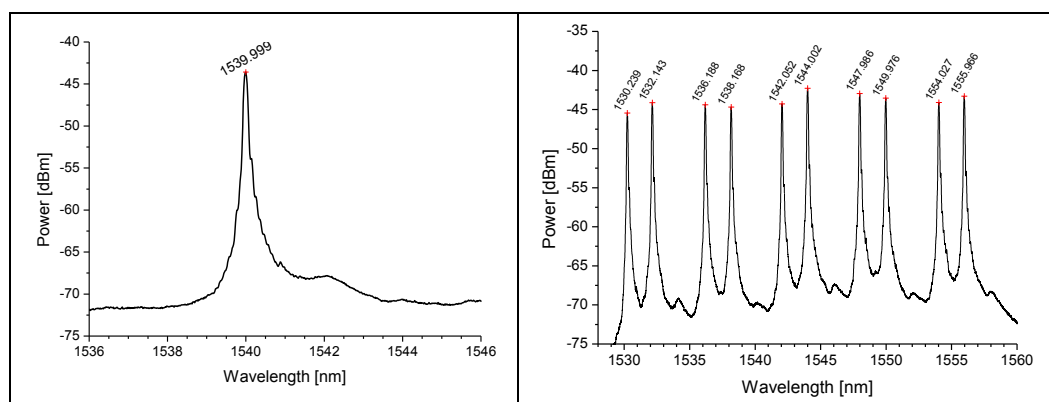


Figure 3: Reflection spectrum (in dB) of a single 63 µm DTG® (left), and 63 µm DTG® array of ten gratings in series (right).

### 1.3 Characterization of the first prototype 60µm Draw Tower FBGs.

#### 1.3.1 Fibre tensile strength

Tensile tests are performed on dummy and sensor fibre to define their ultimate fibre stress ( $\epsilon_{ult}$ ) and ultimate strain at breakage ( $\epsilon_{ult}$ ). In Table 1, it is shown that the ultimate tensile properties of the 60 µm versions are excellent compared to the commercially available 125 µm and 80 µm DTG®s.

Table 1: Statistics on the maximal applied force, the calculated tensile strain and tensile strength of the 63 µm DTG®-fibre in comparison with the commercial 125 µm and 82 µm DTG®-fibre and dummy 62 µm fibre.

Fibre	$F_{max}$ [N]	$\epsilon_{ULT}$ [%]	$\sigma_{f,ULT}$ [MPa] (mean)
125 / 190 µm (DTG®) (N=5)	58.0 ± 4.6	6.3 ± 0.50	4566 ± 362
82 / 114 µm (DTG®) (N=15)	25.3 ± 0.8	6.5 ± 0.21	4667 ± 150
62 / 106 µm (dummy) (N=14)	16.9 ± 0.3	7.4 ± 0.14	5316 ± 99
63 / 106 µm (DTG®) (N=15)	17 ± 0.3	7.4 ± 0.11	5349 ± 78

#### 1.3.2 Strain gauge parameter:

In this research, we are defining the logarithmic relationship between the wavelength shift and applied longitudinal strain by determining a wavelength independent gauge factor,  $S_\epsilon$  which is defined as

$$S_\epsilon = \ln \frac{\lambda_B}{\lambda_{B,0}} \cdot \frac{1}{\Delta \epsilon_3}, \quad (1)$$

with  $\lambda_{B,0}$  the reference or initial Bragg wavelength (e.g. at zero load) and  $\lambda_B$ , the wavelength at any given time. Equation (1) is derived from the well-known standard Bragg condition ( $\lambda_B = 2\bar{n}\Lambda$ ), with  $\bar{n}$  the effective refractive index of the fibre and  $\Lambda$  the period of the grating. In contrary to the linear strain sensitivity commonly used in literature (typical 1.2pm/µε for 1550nm range), the gauge factor,  $S_\epsilon$  according to Equation (1) is applicable for gratings at any given wavelength, moreover it can be used for large wavelength shifts (i.e. for high strain levels). The individual  $S_\epsilon$  factor is determined for several DTG® arrays with multiple gratings in series. The fibre is fixed to translation stages and strained up to more than 0.5% in steps of approximately 800 µε. The DTG® its wavelength is recorded and plotted as a logarithmic, and divided by its initial Bragg wavelength at zero loading,  $\lambda_{B,0}$ , against the applied strain (Figure 4).

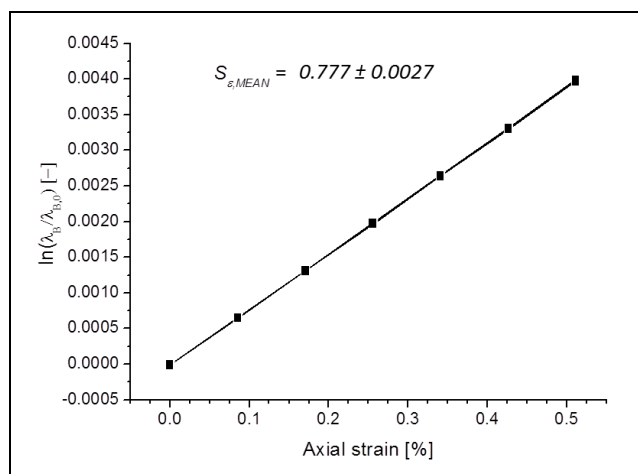


Figure 4: Typical strain calibration curves of ten 63µm DTG®s with the average gauge factor.

In total two arrays with ten 63 µm DTG®s were calibrated. The average strain gauge factor is found  $S_{\epsilon, 63} = 0.777 \pm 0.0027$ . This value matches very well the strain gauge factors of commercially available 80 µm and 125 µm DTG®s. The  $S_{\epsilon}$ -factor will be used further to estimate the strain during automated fibre placement (see Section 2).

### 1.3.3 Temperature sensitivity:

According to literature [2], best fits of the temperature calibration curves for FBGs are obtained using second order polynomials. For the fits of the calibrations performed on the 63µm DTG®s the following quadratic function is used:

$$\ln \frac{\lambda_B}{\lambda_{B,ref}} = S_{T1} \Delta T + S_{T2} \Delta T^2, \quad (2)$$

With  $\Delta T = T - T_{ref}$  the temperature difference between the reference temperature and actual temperature,  $S_{T1}$  and  $S_{T2}$  the wavelength independent linear and quadratic temperature sensitivities, respectively,  $\lambda_{B,ref}$  the Bragg wavelength at the reference temperature,  $T_{ref}$  and  $\lambda_B$  is the measured wavelength at the actual temperature  $T$ . The temperature sensitivities,  $S_{T1}$  and  $S_{T2}$ , are determined by performing a temperature calibration and fitting the calibration curve by using a second order polynomial.

Three samples were prepared for the temperature calibration. The coating of the DTG®s is removed to avoid humidity effects during calibration and each sensor is protected using a quartz capillary which is fixated and sealed using small drops of adhesive. The temperature calibration is performed using a Fluke 9170 metrology well calibrator. The metrology well has a temperature stability of  $\pm 0.005^\circ\text{C}$  and an accuracy of approximately  $\pm 0.014^\circ\text{C}$ . The temperature is cycled twice from  $-22.5^\circ\text{C}$  up to  $135^\circ\text{C}$  in steps of  $22.5^\circ\text{C}$ , see Figure 5, left. The second cycle is used to calibrate the sensors. Each temperature level is kept constant for approximately 30 minutes and the peak wavelength of all samples is continuously recorded. An example of the experimental calibration curve is shown in Figure 5, right. A polynomial (Equation (2)) is fitted to the data points to determine  $S_{T1}$  and  $S_{T2}$ . The calibrated average temperature sensitivity is found to be  $S_{T1} = 6.37\text{E-}6$  and  $S_{T2} = 7.3\text{E-}9$ . Again the values match very well the temperature sensitivities of commercial available 125 µm and 80 µm DTG®s. These parameters can be used to perform temperature compensation techniques or even be used to calculate temperature using the inverse of Equation (2).

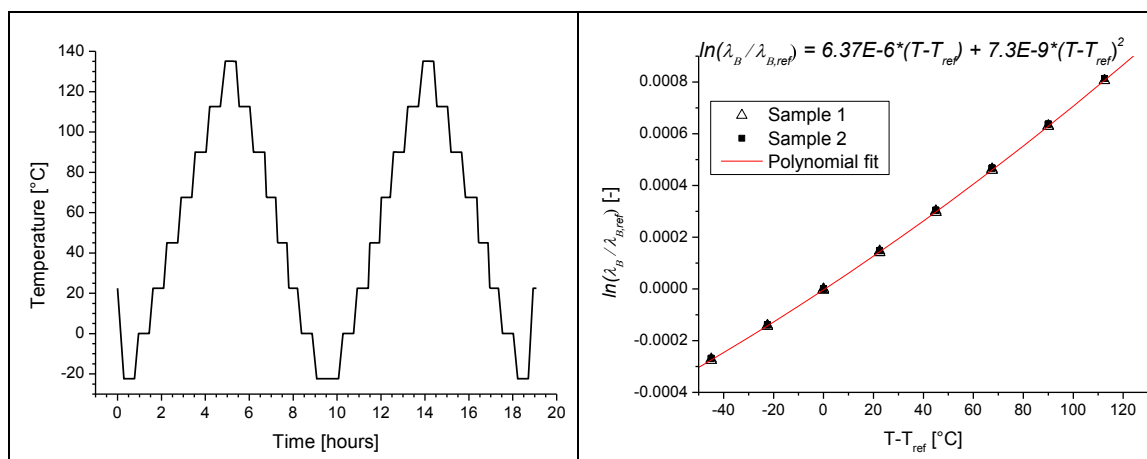


Figure 5: Temperature calibration cycles from  $-22.5^{\circ}\text{C}$  –  $135^{\circ}\text{C}$  (left), calibration curve for three  $63\ \mu\text{m}$  DTG@s fitted polynomial, with  $T_{\theta} = 22.5^{\circ}\text{C}$  (right).

## 2 AUTOMATED FIBRE PLACEMENT

The scope of this part of the workpackage within the SMARTFIBER project is to study automated fibre placement (AFP) using a robot cell of Airborne Technology Centre with a dedicated AFP head and the newly developed  $63\ \mu\text{m}$  DTG@-fibre described in this paper. Specific sensor arrays with a double DTG@ configuration are produced for the tests. The distance between the two DTG@ sensors is 40mm. The aim is to determine the reproducibility of the AFP process. Multiple tests are performed to investigate the impact on the fibre during placement and the strain development is monitored during lay-down of the fibre onto prepreg material and during composite curing.

### 2.1 AFP straight on prepreg

In this test, the optical fibre is manually spooled on the OF reel and then automatically laid down on a GFRP prepreg using the AFP robot with dedicated AFP head (Figure 6, left). A nominal compaction pressure of 1.75bar is used to press the fibre into the prepreg (Figure 6, right). The strains of both sensors are simultaneously monitored during lay-down.

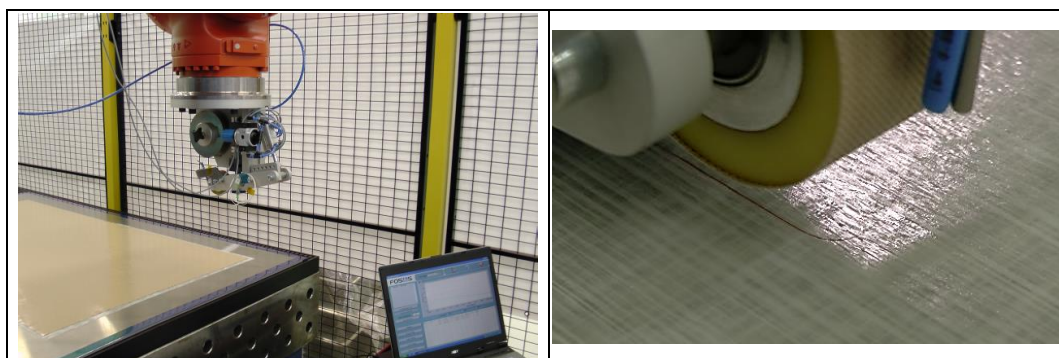


Figure 6: Robot with AFP head and monitoring system (left), close-up of the compaction wheel and optical fibre on prepreg layer after lay-down (right).

The different sequences during the test are clearly shown in Figure 7, the strain develops I) during manually spooling, II) during automated placement and III) during lay-down. The two DTG@s measure a pre-strain of approximately  $400\ \mu\text{strain}$  after lay-down. Two different tests were then performed, each repeated three times: “short trajet tests” with a fibre length of  $\sim 0.2\text{m}$  and “long trajet tests” with a fibre length of  $\sim 1.5\text{m}$ .

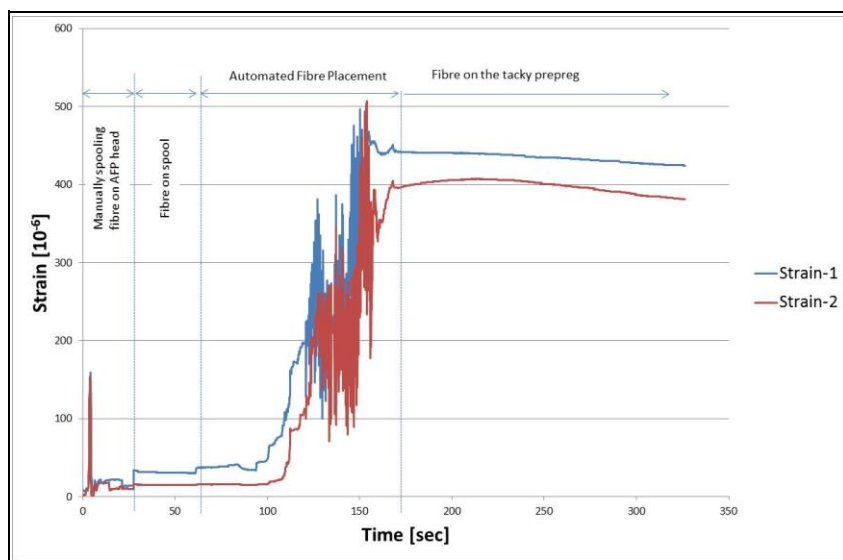


Figure 7: Strain development of two 63µm DTG@s ( $\Delta l=4\text{cm}$ ) during AFP.

All test show that the sensors measure maximum approximately 400 - 600µstrain during lay-down. The value is acceptable and far below the limit of 7% strain at breakage, so these tests show that with the present AFP setup the risk of breaking the optical fibre is very low. In addition, this small pre-strain is beneficiary for keeping the fibres straight after placement. Examples of the results for both tests are shown in Figure 8:

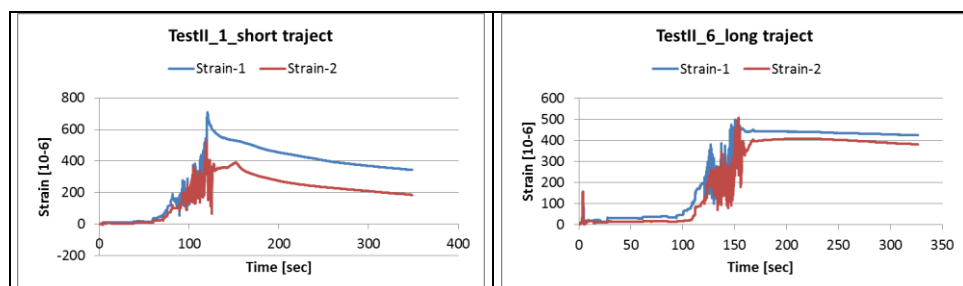


Figure 8: Strain development during lay-down of a 63µm DTG@s pair ( $\Delta l=4\text{cm}$ ) for a short traject (left) and longer traject (right).

We see that for shorter fibre the pre-strain developed during lay-down decreases faster than in the case of longer fibre. We also notice that the strain difference between the first and second sensor is higher for the shorter fibre length. As a consequence, to ensure and control similar pre-strain levels for the sensors and to keep the initial pre-strain after lay-down, the length of the fibre after the sensors should be taken long enough. Results of further tests show that both sensors have exactly the same pre-strain and that the drop of pre-strain evolves much slower if compaction pressure is increased to 6bar. The work performed up to now has only focused on placement of straight fibres. In a second stage a curved path will be envisaged.

### 2.1.1 Strain measurements during lay-down, lay-up, curing and after consolidation

In a final test, two fibres, having 1 DTG@s, are embedded in a GFRP composite (0.6m x 1.5m) with lay-up  $[0,90]_s$ . The laminate was oven cured at 120°C and vacuum is applied during curing. Both sensors were monitored at several stages during the embedding and production process, starting from fibre lay-down using AFP (compaction 6bar), after final lay-up, during application of vacuum, and finally after curing (Figure 9). A very similar response is found for fibre 1 and 2. The strain

values of fibre 1 at different time stamps during the production process, is shown in Figure 9, right. A small decrease is noticed after composite lay-up, which is caused by a release of pre-strain during the time between AFP and finalization of the bagging material (~15minutes).

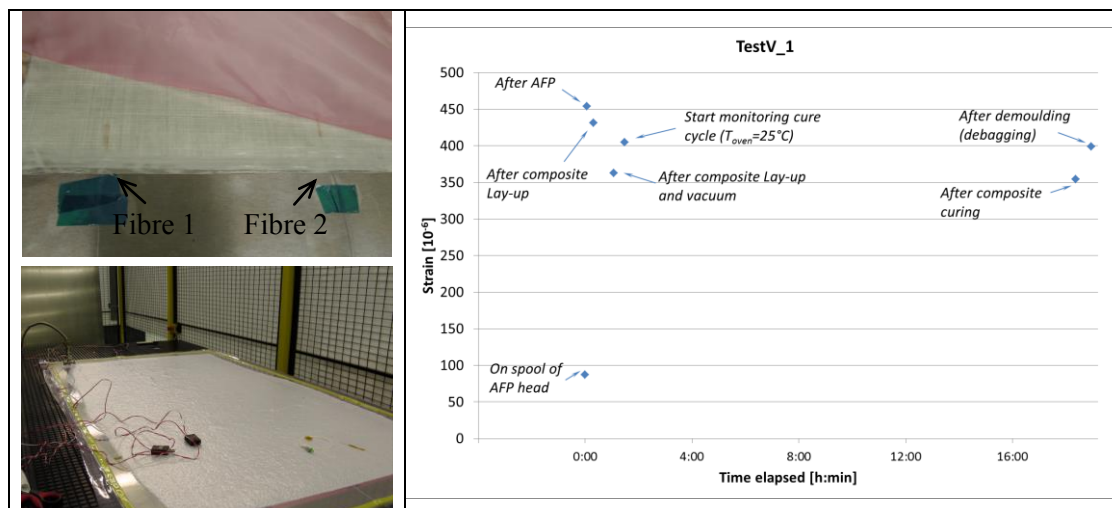


Figure 9: Optical fibre egress points with PTFE tubes in final lay-up (left), lay-up in vacuum bag (right)

More than 90% and 75% of pre-strain is left for fibre 1 and fibre 2, respectively. The strain after application of vacuum has dropped as well, which is probably a combination of compaction of the layers and drop in temperature because of air flow. Note that the strain level after debagging compared to the strain level measured at the start of the cure cycle ( $T=25^{\circ}\text{C}$ ), are found to be very similar. This could indicate that for this specific GFRP material no significant residual strain is built up during its production process.

## CONCLUSIONS

In general it can be concluded that the newly developed smaller diameter fibre and draw tower FBG prototype with cladding  $63\ \mu\text{m}$  and coating outer diameter  $106\ \mu\text{m}$ , has identical sensor properties compared to the commercial available DTG®s. Moreover the strain at breakage is found excellent and the fibre copes very well with the AFP process. The induced strains are very small and form no risk to fibre breakage and fibre placement tests show to be very repeatable. We are able to control the pre-strain during embedding and assure straight fibre alignment. Result of these test prove that automated fibre embedding is feasible, even with very thin optical fibre sensors.

## ACKNOWLEDGEMENT

The research leading to these results has received funding from the European Union Seventh Framework Programme FP7/2007-2013 under grant agreement n° 257733 (SmartFiber)

## REFERENCES

- [1] Trademark of FBGS-technologies GmbH, more information available from <http://www.fbgs.com>
- [2] Pal, S., Sun, T., Grattan, K.T.V., Wade, S.A., Collins, S.F., Baxter, G.W., Dussardier, B., and Monnom, G., *Non-linear temperature dependence of Bragg gratings written in different fibres, optimised for sensor applications over a wide range of temperatures*. Sensors and Actuators a-Physical, 2004. **112**(2-3): p. 211-219.